2013 IEEE/RSJ International Conference on
Intelligent Robots and Systems (IROS)
November 3-7, 2013. Tokyo, Japan

Mechanics-Based Kinematic Modeling of a Continuum Manipulator

Yang Wenlong, *Student Member*, *IEEE*, Dong Wei, *Member*, *IEEE* and Du Zhijiang, *Member*, *IEEE*

***Abstract*—A continuum manipulator with triangular notches is proposed for the potential medical applications, which is driven in the plane by wires embedded in bilateral symmetry channels. The focus of this present research is a mechanics-based kinematic model of the proposed continuum manipulator using the Timoshenko beam theory to map the driven load to the manipulator shape. In the proposed model, the continuum manipulator is divided into several V-shape units, each of which consists of two 2-node Timoshenko beam elements. Compared with previous approaches, our proposed model discards the constant curvature approximation, in which the distributed force caused by the interface contact between the wire and the V-shape unit is also considered simultaneously. The proposed mechanics model is validated experimentally on a segment of Nitinol flexible manipulator, which illustrates the effectiveness of our model to describe the continuum manipulator shaping.**

I. Introduction

Continuum arms can be defined as continuously curving manipulators with flexible structures or joints, which exhibit marvelous behaviors similar to biological trunks, tentacles and snakes etc [1-2]. Continuum arms, also known as hyper-flexible, hyper-redundant, and continuous backbone robot arms, have attracted more attention from variety of fields, especially in medical applications due to their incredible characteristics for continuously bending, infinite degree of freedom, and dexterity in constrained environments. In contrast to rigid links and joints, the continuum manipulator is ideal for surgeon operation in constrained environments, which offers some distinctive features such as inherent compliance, reduced weight, fault tolerance, and whole arm manipulation capability. Those features have also naturally inspired researchers to develop continuum robots for minimally invasive surgery (MIS), such as single port abdominal surgery (SPAS) and natural orifice transluminal endoscopic surgery (NOTES) [3-6]. Compared with the traditional MIS systems, the SPAS and NOTES minimize the incision trauma and shorten the recovery time. Recently, more generic SPAS and NOTES robots based on continuum design have been proposed for the applications of prostatectomy, cholecystectomy, fetal surgery, and endoscopic diagnosis and intervention, et al [7-15].

The characteristic of continuum arms challenge the developing and formulating the kinematic model. In contrast to rigid-link robots, the kinematic model and mechanics model of the continuum robot are coupled. Consequently, the kinematic modeling of continuum robots cannot be formulated solely in terms of constrained motion between rigid bodies, but must also incorporate deformation modeling of elastic components. Recently, some mechanics models have been established for continuum robots. Jones and Walker [9] developed a modular kinematic framework for a multi-section elephant trunk robot, which enables real-time task and shape control by relating workspace coordinates to actuator inputs. This approach also considers physical manipulator constraints. Dupont et al [10, 11] developed a multi-tube quasistatic model of concentric tube robot with external loads to robot shape and tip configuration. In their approach, the continuum robot is modeled as a single Cosserat rod with properties along its length corresponding to the composite stiffness and initialized curvatures of the unloaded robot. Trivedi et al [16] used the Cosserat rod theory to derive the continuum robot's deflection which is subject to the external loading. Webster et al [17, 18] presented a mechanics model based on Bernoulli Euler beam for a concentric tube continuum robot, in which the torsional effects were added to the modeling framework in straight transmissions. Xu and Simaan [12] demonstrated intrinsic force sensing capabilities of a flexible multi-backbone continuum robot, using screw theory to analyze the limitations and provide geometric interpretation to the sensible wrenches. Camarillo et al [19] presented a new linear model for transforming desired beam configuration to tendon displacements, and the distributed force caused by tendon along the length of the tendon-beam interface was also considered. In some models mentioned above, the piecewise constant curvature approximation is employed, and the distributed force generated by the tendon, wire and cable is neglected. However, it is obvious that the piecewise constant curvature assumption is not sufficient for precision modeling and real-time controlling, especially when torsion, lateral force, external forces and moments are applied [20].

This paper presents a novel continuum manipulator which is constructed from a Nitinol tube with triangular notches and driven in the plane by wires. This paper is mainly focused on a new mechanics-based model mapping between driven wire tension and arm shape. The model is essential in kinematic modeling and controlling the manipulator accurately in future, and can be applied to other continuum manipulators with similar notched structure. In the proposed model, the deflection profile of the continuum manipulator is not subject to the constant curvature approximation and the distributed force caused by the driven wire is considered simultaneously.

The structure of this paper is as follows. Section II presents the overview of the continuum manipulator which provides a large hollow lumen for driven wires, power and signal cables of end micro-instruments. Section III introduces the mechanics model of the continuum manipulator based on Timoshenko's beam model. Section IV discusses the kinematic model based on the mechanics model. Finally, the proposed model is experimentally validated in Section V and the article is concluded in Section VI.

* All the authors are with the State Key Laboratory of Robotics and System, Harbin Institute of Technology, Harbin, China, 150080 (Corresponding author, Du Zhijiang, Phone: 86-451-86403362, Fax: 86-451-86403613, e-mail: duzj01@hit.edu.cn).

II. Continuum Manipulator Design

A. Design Consideration

Minimally invasive medical procedures involve the manipulation of tools, sensors and endoscopic devices inside the body while minimizing damage to surrounding anatomical structures. The requirements for different surgery performances are different, although all actions are required to be implemented in confined space, so the DOF (Degree of Freedom) of robot system must be enough to meet the MIS requirements. The continuum manipulator arm is a good choice in confined cavity compared to the traditional link-joint systems, which can achieve large scale deformation but is difficult to manipulate. In order to fulfill the MIS tasks, the robot should be a foldable system, be able to pass through a small incision, and operate the target organs and involved tissues with enough precision and force. In addition, the translational workspace should be able to be limited within 50mm×50mm×50mm [7].

The design objective of the continuum arm is to determine the position of the tip-tool and the dimension of the lumen for actuation and sensing. Design requirements include, enough degree of freedom for tool manipulation and exploration, compact size for insertion through incision, high dexterity of manipulation, and geometry extensible to fit various size of components.

B. Manipulator Design

According to medical constrains, a 30-35mm incision is available for laparoscopic operations [14], so a design of the continuum manipulator with 10mm diameter is acceptable. The proposed continuum manipulator is driven by wires which pass through bilateral symmetry channels of Nitinol tube (shown in Fig 1). One end of the wires is fixed at the top of the tube and the other end is connected to the actuation motors to steer tightening or loosening the wires. When tension is applied on the wires, the flexible tube will bend naturally. The proposed flexible manipulator arm can achieve one-DOF bending motion in plane by alternating two wires' tightening and loosening. Fig. 1 shows two segments can be stacked to be configured as two-DOF continuum snake-like arm, and the two bending planes are perpendicular to each other, i.e. the bending plane of one segment is the neutral plane of the other one. The driven-wire is fixed on the top frame of each segment, which causes the second segment driven-wire passing through the first segment. Since the driven-wire plane of first segment is identical to the neutral plane of second segment, the deformation of these two segments is decoupled. In our design of the notches arm, the arm only can be bended to the direction of opening and closing of the triangular notches, so the influence caused by the torsion and driven-wire force of the distal segment to the base segment can be neglected. In addition, the continuum manipulator features a large lumen to house support disks, additional driven wires for instruments, and sensor cables etc. In our proposed design shown in Fig. 1(a), the notches are identical, equally spaced, and interleaved, which are cut by the slow wire EDM. For the proposed flexible manipulator, the maximum bending angle θ_{max} depends on the key geometric and physics variables, i.e. the notch angle $\boldsymbol{\alpha}$, the notch number $\boldsymbol{N}$, the notch overlap, and material properties etc.

$$\theta_{\max} = N\alpha \tag{1}$$

It can be seen that even though this paper focuses on a planar model of single segment, the work discussed and the approach outlined in this paper is generic, which can be further used into the full three-dimensional model of notched multi-segment and geometry optimization to enhance the system property with optimal design variables.

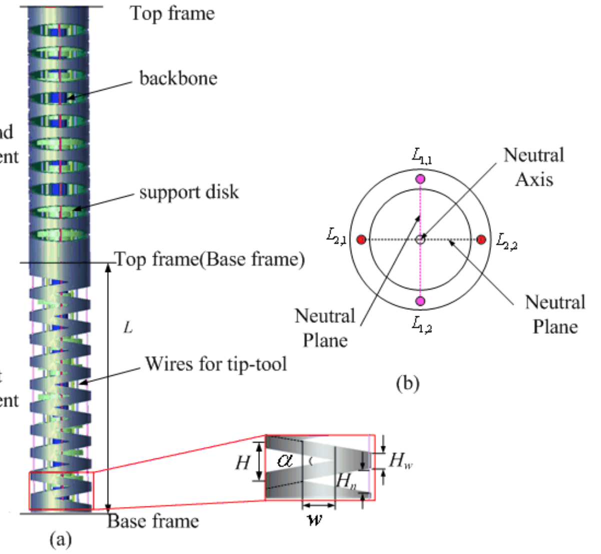

Fig. 1 (a) Solid continuum arm model of two segments. (b) Connecting frame.

III. Mechanics Modeling

A. Mechanics Model of the Flexible Arm

As shown in Fig. 2, the whole structure can be divided into several individual V-shape units, in order to establish the framework for the mechanics-based model of the flexible arm. The Fig. 2 (b) shows the contact interface between the V-shape segment and the driven wire. If the concerned part shown in Fig. 2 (b) is separated from the structure, a force balance can be formulated, in which the tension force F_T (with α_1 and α_2 respectively) and the distributed contact force F_w are involved.

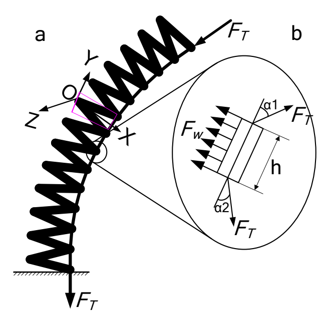

Fig. 2 The segments of the flexible manipulator arm in the bending plane and the forces applied on the V-shape unit.

It can be seen that a V-shape segment can be considered as a combined structure with two rings. It is obvious that the stiffness of the overlap area is relatively high, so the deformation mainly concentrated in the beam segments between the overlaps of the triangular notches, as shown in Fig.

3. It also should be noted that the deformed segment is a part of an arc structure with small central angle, so it can be simplified as two straight beams. As shown in Fig. 3, the blue straight beam and the orange arc segment are hypothesized as identical structures, which are the main deformation area.

In our design, the thickness and the length are 0.6 mm and 1.67 mm respectively, so the slenderness ratio (slenderness ratio is defined as ratio of the length of beam to cross section) of beam A and beam B is relatively small. Therefore, the mechanics model of the beam should be formulated based on 3-dimensional 2-node Timoshenko beam model rather than Euler-Bernoulli beam. As shown in Fig. 3, each arc beam of the V-shape unit is divided into two 2-node Timoshenko beam elements. The global coordinate system *O-XYZ* is assigned in the left corner of the V-shape unit, and the *O-XY* is the bending plane. For the separated beam A and B, the local coordinate system O_i-$U_iV_iW_i$ and O_j-$U_jV_jW_j$ can be assigned respectively. Beam A and B have identical geometry properties, and share the same node *j*. To facilitate the coordinate transformation, O_i and O_j locates at the centroid of the left sections of beam *A* and beam *B* respectively. *U*-axis′ and *V*-axis′ positive direction is along element axis from the left node to the right one.

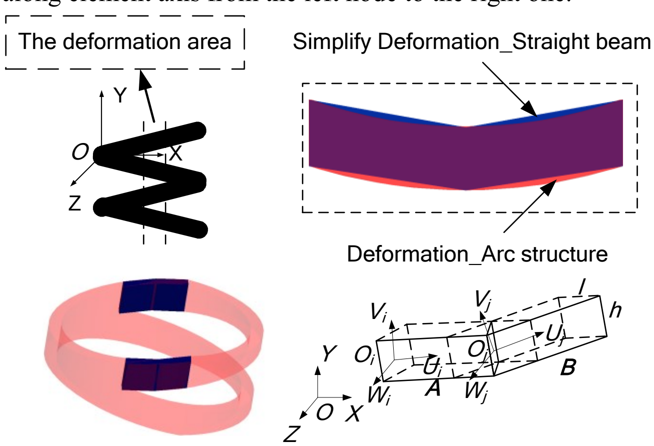

Fig. 3 Analysis of V-shape unit and coordinate assignment.

B. Stiffness Model

For a 3-dimensional 2-node Timoshenko beam element, there are 12 displacement components consisting of 3 linear displacements *x*, *y*, *z* and 3 angular displacements θ_x, θ_y, θ_z in node *i* and node *j* respectively, as shown in Fig. 4. The stiffness matrix of a 3-dimensional 2-node Timoshenko beam element can be derived based on consistent shape functions [21].

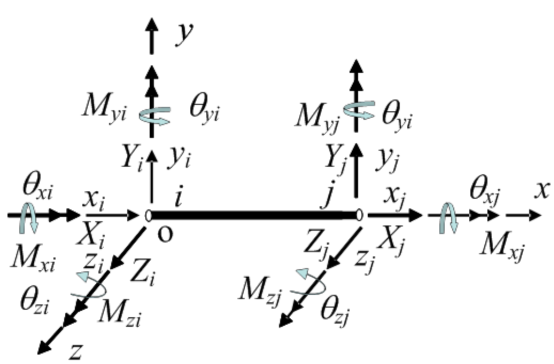

Fig.4 Nodal forces and nodal displacements of Timoshenko beam in local coordinate system.

There are three forces and three moments for each node (*i* and *j*) corresponding to three linear displacements and three rotational displacements respectively. The node force vector and displacement vector in the local coordinate system can be formulated as follows.

$$\overline{P} = [\overline{P_i}\ \overline{P_j}] = [X_i\ Y_i\ Z_i\ M_{xi}\ M_{yi}\ M_{zi}\ X_j\ Y_j\ Z_j\ M_{xj}\ M_{yj}\ M_{zj}]^T \tag{2}$$

$$\overline{D} = [\overline{D_i}\ \overline{D_j}]^T = [x_i\ y_i\ z_i\ \theta_{xi}\ \theta_{yi}\ \theta_{zi}\ x_j\ y_j\ z_j\ \theta_{xj}\ \theta_{yj}\ \theta_{zj}]^T \tag{3}$$

Then the stiffness model of the beam can be established as below,

$$\overline{P} = \overline{K} \cdot \overline{D} \tag{4}$$

where $\overline{P}$, $\overline{K}$ and $\overline{D}$ are the nodal load vector, nodal stiffness matrix, and nodal displacement in the local coordinate system, respectively. The elements in the nodal stiffness $\overline{K}$ matrix can be expressed based on material properties and structural parameters. Normally, the stiffness matrix in the global coordinate system can be expressed as follows,

$$K = T^T \overline{K} T \tag{5}$$

where *T* is the transformation matrix based on the direction cosine matrix from the local coordinate to the global coordinate.

$$T = \begin{bmatrix} T_A & 0 & 0 & 0 \\ 0 & T_A & 0 & 0 \\ 0 & 0 & T_B & 0 \\ 0 & 0 & 0 & T_B \end{bmatrix} \tag{6}$$

where T_A and T_B are the direction cosine matrix of the two Timoshenko elements shown in lower right corner of Fig. 3.

Finally the stiffness model in the global coordinate system can be formulated as below,

$$P = K \cdot D \tag{7}$$

where *P*, *K* and *D* are the nodal load vector, stiffness matrix, and nodal displacement in the global coordinate system, respectively.

C. Mechanics Model of Single V-shape Unit

As shown in Fig. 5, each V-shape unit consists of upper and lower segments, and each segment is composed of two Timoshenko beam elements, therefore other parts are considered as rigid bodies. For the flexible segments *i-j-k* or *d-e-f*, as mentioned above, two beams (*i-j* and *j-k* or *d-e* and *e-f*) are used in discussion with the shared node *j* or *e*. As shown in Fig. 5, the external load F_T acts longitudinally at the distal tip and the distributed load normal to the curvature of the beam acts on the interface between the wire and the beam. *M* is the moment acting on the node *k* and *d*, and L_1 and L_2 are the length of Timoshenko element and assumed rigid body respectively.

The stiffness matrix of beam with two Timoshenko beam elements and three nodes can be formulated in the global coordinate system by integrating the stiffness matrices of the Timoshenko beam *i-j* and *j-k* according to the diagonal superposition principle,

$$K_a = \begin{bmatrix} k_{11}^A & k_{12}^A & 0 \\ k_{21}^A & k_{22}^A + k_{11}^B & k_{12}^B \\ 0 & k_{21}^2 & k_{22}^B \end{bmatrix} \tag{8}$$

where K_a, K_{ij}^A, K_{ij}^B, are the assembly stiffness of upper beam in V-shape unit, sub-block stiffness matrix of beam *A* and B in Fig. 3, respectively. The subscripts with *i* and *j* present the index of node in each Timoshenko element respectively.

When the load-displacement relationship of node j, k and d, e is investigated, the lower right corner 12-dimensional matrix of K_a can be chosen as a new stiffness matrix K_u in the following discussion.

$$\mathrm{K}_u = \begin{bmatrix} k_{22}^A + k_{11}^B & k_{12}^B \\ k_{21}^2 & k_{22}^B \end{bmatrix} \tag{9}$$

Since the geometric of upper and lower combined beam are identical, the stiffness of upper and lower beam is the same. The stiffness matrix of single V-shape combined beam element can be expressed as follows.

$$K = \begin{bmatrix} K_u & 0 \\ 0 & K_u \end{bmatrix} \tag{10}$$

Therefore, the displacement of upper and lower beam in the V-shape unit can be solved as below via the stiffness equation in the global coordinate.

$$P = K_u \cdot D \tag{11}$$

The distributed load is considered on the i^{th} V-shape unit, which is applied on the upper beam. When the $(i+1)^{th}$ distributed load is considered, it is also discussed on the upper beam of the $(i+1)^{th}$ V-shape unit. Since the deformation occurs on the notches deformed area (i-j-k and d-e-f), the force can be moved from node a to node k. The force vector of upper and lower combined beam element is shown as below,

$$P = \begin{bmatrix} P_u & 0 \\ 0 & P_l \end{bmatrix} \tag{12}$$

where the P_u and P_l contain six force elements and six moment elements acting on the upper and lower combined beam element respectively. Since the driven force is parallel to the deformation plane, the force and moment acting on the node k and node d are not zero, which include the driven force in X and Y direction (F_x, F_y) and the driven moment (M).

With the equation (10), (11), (12), the displacement of every node in each combined Timoshenko beam of the V-shape unit can be calculated. Displacement vector of upper and lower combined beam element is expressed as follows.

$$D = \begin{bmatrix} D_u & 0 \\ 0 & D_l \end{bmatrix} \tag{13}$$

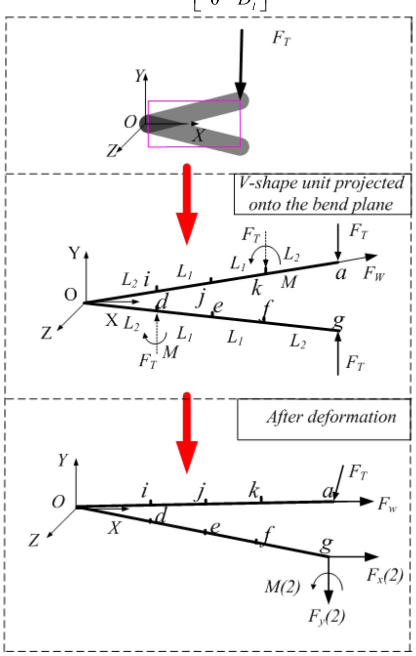

Fig. 5 Force analysis of upper and lower beam segment's combinations.

The θ_{wk} and θ_{wd} in the displacement vector D represent the deformation angle of node k and node d. θ_{wk} and θ_{wd} are the same direction (clockwise or anti-clock wise) in the global coordinate, so the bending angle of the single V-shape unit can be formulated as below.

$$\theta_{kd} = |\theta_{\mathrm{wd}}| + |\theta_{\mathrm{wk}}| \tag{14}$$

Considering the balance of the wire in the contact area, the bending angle θ_{kd} can also be calculated as below.

$$\theta_{kd} = f(F_w) \tag{15}$$

It can be hypothesized that when the flexible manipulator arm is deformed, the wire is under a balance condition, therefore the contact force Fw can be formulated as below.

$$F_w = F_T \cdot (\sin(\theta_{kd}) \tag{16}$$

Generally, the process for θ_{kd} solving includes five steps, in which iterative approach is employed.

- Firstly, F_w is zero, and based on that to solve $\theta_{kd}(1)$.
- Secondly, according to equation (15), F_w of first step can be calculated.
- Thirdly, according to the (10)-(12), to solve θ_{kd} (i) and calculate the error with the consideration of F_w in the second step. The error is shown as follows

$$\Delta\theta_{\omega k} = \theta_{\omega k}(i+1) - \theta_{\omega k}(i)(i \to \infty) \tag{17}$$

- Then the X and Y direction force and moment generated on node a after deformation can be formulated as below.

$$\begin{aligned} F_x(i) &= F_T \cdot \sin(\theta_{kd}) + F_w(i) \cdot \cos(\theta_{kd}) \\ F_y(i) &= F_T \cdot \cos(\theta_{kd}) + F_w(i) \cdot \sin(\theta_{kd}) \\ M\_a(i) &= Fy(i) \cdot L2 \cdot \cos(\alpha) - Fx(i) \cdot L2 \cdot \sin(\alpha) \end{aligned} \tag{18}$$

- Finally, to evaluate the value of the error. If the value is not equal to zero, repeat the second step to the fourth step until $\Delta\theta_{kd}$ is zero, i.e. the single V-shape unit and the driven wire are all under balance condition.

After the single V-shape unit bending is discussed, we can write the static equilibrium equations and solve the reaction force $F_y(2)$, $F_x(2)$ and moment $M(2)$ shown in Fig. 5, which are the initialized force and moment for the second V-shape unit respectively.

$$\begin{aligned} Fy(2) &= F_T \cdot \cos(\theta_{kd}) - F_w \cdot \sin(\alpha - \theta_{kd}) \\ Fx(2) &= F_T \cdot \sin(\theta_{kd}) - F_w \cdot \cos(\alpha - \theta_{kd}) \\ M(2) &= F_y(2) \cdot L\_y - F_x(2) \cdot L\_x \end{aligned} \tag{19}$$

L_y and L_x is the moment arm of node a of second V-shape unit in X and Y axis that is caused by the first V-shape unit deformation, can be expressed as follows respectively.

$$\begin{aligned} L\_y &= (H \cdot \sin(\theta_{kd}) + (2 \cdot L1 + L2) \cdot (\cos(\alpha - \theta_{kd}) - \cos(\alpha))) \cdot \cos(\theta_d) \\ L\_x &= (H \cdot \cos(\theta_{kd}) + (2 \cdot L1 + L2) \cdot (\sin(\alpha) - \sin(\alpha - \theta_{kd}))) \cdot \cos(\theta_d) \end{aligned} \tag{20}$$

The essential results of the analysis for the single V-shape unit are (13) and (18), with which the mechanics mode for single V-shape unit is established.

D. Mechanics Model of the Flexible Manipulator Arm

As mentioned above, the flexible manipulator arm is divided into several V-shape units, so the mechanics model of the continuum arm is based on the model of single V-shape unit. The global coordinate system O_0-$X_0Y_0Z_0$ is assigned on the right point of base platform, shown in Fig. 6(a). The mechanics-based model of each V-shape unit is investigated respectively, and the bending angle of the flexible manipulator arm can be derived based on deformation of each individual V-shape unit. The stiffness matrix of every Timoshenko combination beam is identical in local coordinate systems. As shown in Fig. 6(*a*), N V-shape units include $2N$ Timoshenko combined beams, in which the index number of V-shape units is started from distal to the base of the flexible arm. $2N$ combined beams are divided into two groups, i.e. odd group (the index number i is odd) and even group (the index number i is even), where N represents the number of the upper and lower beam.

The direction of external force and the additional moment of the i^{th} combined beam are changed due to the deformation of beams from 1 to i-1, shown in Fig. 6(*a*). When the deformation of continuum arm is discussed, the force vector P_u in (12) and the corresponding displacement vector D_u of two node in each upper and lower combined beam can be simplified as follows, the forms of which are identical with the P_l and D_l.

$$\begin{aligned} P_u &= [0\ 0\ 0\ 0\ 0\ 0\ F_x\ F_y\ 0\ 0\ 0\ M+M_1]^T \\ D_u &= [u_1\ v_1\ w_1\ \theta_{u1}\ \theta_{v1}\ \theta_{w1}\ u_2\ v_2\ w_2\ \theta_{u2}\ \theta_{v2}\ \theta_{w2}]^T \end{aligned} \tag{21}$$

where F_x, F_y, and $M+M_1$ are the external force and moment acting on the node k and d of each V-shape unit as shown in Fig. 6, and the vector form of beam in each V-shape unit is identical. The moment is composed two parts, i.e. the moment on node a (M), and the moment caused by the force transferring from node a to node k and node d (M_1). As shown in Fig. 6, after the deformation the i^{th} V-shape unit will induce strong effects on the initialized force and moment of the $(i+1)^{th}$ V-shape unit. According to the (14), the total bending angle consists of i V-shape units ($2 \leqslant i \leqslant N$) can be formulated as follows, the right and left bending angle are equal in solving the total bending angle,

$$\theta\_sum(i) = \sum_{n=1}^{n} \theta_{kd}(n) = \sum_{n=1}^{i} (\theta_{wk}(n) + \theta_{wd}(n)) \tag{22}$$

where the θ_{kd}(n) is the bending angel of each V-shape unit calculated via the load-displacement equation. The θ_{wk}(n) and θ_{wd}(n) is the bending angle of upper beam and lower beam in the i^{th} V-shape unit respectively.

In the proposed model, the initialized force and moment acting on the node a of the i^{th} V-shape unit can be solved according to the $(i-1)^{th}$ V-shape unit. The deformation of the first V-shape unit has been calculated in previous section, so the force and moment acting on the node a of each V-shape unit can be formulated as follows,

$$\begin{aligned} Fy(i) &= F_y(i-1)\cdot\cos(\theta_{kd}(i-1)) - F_x\cdot\sin(\theta_{kd}(i-1)) + F_w(i)\cdot\sin(\theta_{kd}) \\ Fx(i) &= F_y(i-1)\cdot\sin(\theta_{kd}(i-1)) + F_x\cdot\sin(\theta_{kd}(i-1)) + F_w(i)\cdot\cos(\theta_{kd}) \\ M(i) &= M(i-1) + F_y(i-1)\cdot L\_y(i-1) + F_x\cdot L\_x(i-1) \end{aligned} \tag{23}$$

where the L_y and L_x presents the moment arm acting on the i^{th} node a by the $F_x(i)$ and $F_y(i)$, which can be formulated as follows respectively.

$$\begin{aligned} L\_y(i) &= H\cdot\sin(\theta_{kd}(i)\cdot\cos(\theta_d(i)) \\ &\quad + (2\cdot L1 + L2)\cdot(\cos(\alpha-\theta_{kd}(i)) - \cos(\alpha))\cdot\cos(\theta_d(i)) \\ L\_x(i) &= H\cdot\cos(\theta_{kd}(i))\cdot\cos(\theta_d(i)) \\ &\quad + (2\cdot L1 + L2)\cdot(\sin(\alpha) - \sin(\alpha-\theta_{kd}(i)))\cdot\cos(\theta_d(i)) \end{aligned} \tag{24}$$

On the other hand, the lateral force F_w is different for different V-shape unit, which is expressed as follows

$$Fw(i) = \begin{cases} F_T\cdot(\sin(\theta_{kd}(i)) & i = 1 \| i = N \\ F_T\cdot(\sin(\theta_{kd}(i)) + \sin(\theta_{kd}(i-1))) & 1 < i < N \end{cases} \tag{25}$$

Since the initialized force should be transferred to node k and node d of each V-shape unit, the force vector for the upper and lower beam in V-shape unit is different. The force vector for upper beam in the i^{th} V-shape unit can be formulated as follows.

$$\begin{aligned} P_u(i) = [&0\ 0\ 0\ 0\ 0\ 0 \\ &F_x(i)\ F_y(i)\ 0\ 0\ 0\ M(i) + (Fy(i)\cdot\cos(\alpha) - Fx(i)\cdot\sin(\alpha))\cdot L2]^T \end{aligned} \tag{26}$$

The force vector for lower beam can be formulated as below.

$$\begin{aligned} P_l(i) = [&0\ 0\ 0\ 0\ 0\ 0\ F_x(i)\ F_y(i)\ 0\ 0\ 0 \\ &-M(i) - (Fy(i)\cdot\cos(\alpha) - Fx(i)\cdot\sin(\alpha))\cdot(2\cdot L2 + L2)]^T \end{aligned} \tag{27}$$

The equation (26) and (27) are substituted into stiffness equation (11) yielding the θ_{kd} of each V-shape unit. Finally, using (22), the total bending angle $\theta\_sum(N)$ can be solved. To achieve the balance of flexible arm and driven wire, the iterative approach is employed for the calculation in each V-shape unit as mentioned above. The model mentioned above maps the beam articulation to the single wire tension. $\theta\_sum(N)$ is the total bending angle of the flexible arm.

IV. Kinematics of Continuum Arm

In the actual applications of the proposed system, the mapping between the distal position and the length of driven wires is very important. For the purpose of controlling and future mechanical optimization, the forward kinematic model of the continuum manipulator arm is built mapping the joint space to the operation space. The flexible arm's deformation is occurred by the deformation of single V-shape unit in a relatively concentrated area between the notches, so the kinematic model is built based on the separate set of points in the relatively concentrated area. The value of the separate points can be derived from a series of kinematic parameters below.

Fig. 6 (b) illustrates the kinematics schematic of 14 V shape units. The frame 0 is the base frame, and the frame i ($i \geqslant 1$) is located at the node k of the i^{th} V-shape unit. The $\{i\}$ represents the right-hand frame with the axis $\{x_i, y_i, z_i\}$.The T_a^b represents the transformation matrix from frame a to b. In the proposed kinematic model, all of V-shape units are considered as independent joints.

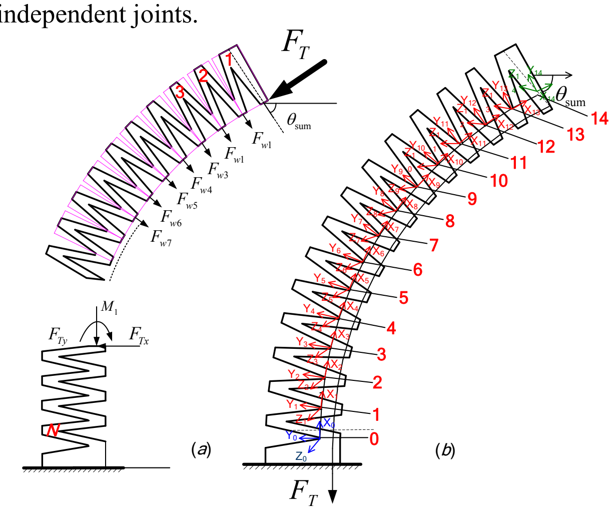

Fig. 6 (a) A representation of the beam index in the mechanics model. (b) Schematic drawing of the continuum arm and the bending arm kinematic. It illustrates the individual joints and the used coordinate axis.

The kinematics model of the bending flexible arm is built modularized, and the D-H kinematic can be applied on each V-shape unit. The D-H table of the continuum arm is presented in Table I. The $\theta_{kd}(i)$ is the bending angle of i^{th} V-shape unit, which can be calculated based on the mechanics model. The l_i is the height of the notch in V-shape unit during the deformation, which can be formulated as follows.

$$l_i = 2\cdot(2L_1 + L_2)\cdot\sin\left(\frac{\alpha-\theta_{kd}(i)}{2}\right) \tag{28}$$

TABLE I. DENAVIT-HARTENBERG TABLE OF THE CONTINUUM ARM

i	1	2	3	…	12	13	14
α_i	0	0	0	…	0	0	0
l_i	l_1	l_2	l_3	…	l_{12}	l_{13}	l_{14}
d_i	0	0	0	…	0	0	0
θ_i	$\theta_{dk}(1)$	$\theta_{dk}(2)$	$\theta_{dk}(3)$	…	$\theta_{dk}(12)$	$\theta_{dk}(13)$	$\theta_{dk}(14)$

The forward kinematic of the continuum arm is computed using the transformation matrix from base frame {0} to the distal frame {14} T_0^{14}

$$T_0^{14} = T_0^1\cdot T_1^2\cdot T_2^3\cdots T_{12}^{13}\cdot T_{13}^{14} \tag{29}$$

The transformation matrix can be formulated as below.

$$T_{i-1}^{i} = \begin{bmatrix} \cos(\theta_{kd}(i)) & -\sin(\theta_{kd}(i)) & 0 & l_i \\ \sin(\theta_{kd}(i)) & \cos(\theta_{kd}(i)) & 0 & 0 \\ 0 & 0 & 1 & 0 \\ 0 & 0 & 0 & 1 \end{bmatrix} \tag{30}$$

The process mentioned above maps distal position to bending angle, and bending angle to tension force respectively. As shown in Fig. 7, the mapping relationship among driven space, joint space and operation space are illustrated, so it can be seen that the mechanics model is the basis of kinematic model when the assumption of constant curve is not used.

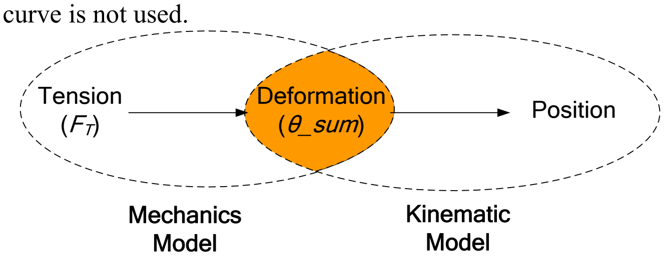

Fig. 7 The diagram of the mechanics model and kinematic model.

V. EXPERIMENTS AND RESULTS COMPARISON

In this section, experiments are performed to validate the proposed mechanics model while changing the wire tension in increments of 1N in [0, 14]. The physical properties of the flexible arm are listed in Table II. The structure's bending experiments are performed on two pieces of Nitinol continuum arm, which consists of 6 V-shape units and 19 V-shape units respectively. Fig. 8 presents the 6 V-shape units flexible manipulator's bending at three different wire tensions (0N, 10N and 14N, respectively) to show the effectiveness of our continuum arm.

In order to observe and measure, a thin metal plate is glued on the top of the flexible manipulator, so the tilting of the plate indicates the bending angle of flexible arm. Since the weight of this thin plate can be neglected, it cannot induce the bending deformation of the flexible arm. Fig. 9 shows the experiment setup for this performance test of the proposed mechanics model. The bending angle is measured by the laser Tracker (Tracker3, API Inc.) via tracking the position of the target ball, the resolution and accuracy of which are $1\mu m$ and $15\mu m$ respectively. The driven tension is generated by the standard weights from 100g to 1400g. For each bending angle, the measurement process is followed by (1) Choose two random points in the bending plane, and record the position of the two target balls (2) Construct the line between the two points via the Tracker3 embedded software. (3) Measure the angle between each constructed line and base line, which also can be implemented via the embedded software. (4) To reduce the man-made measurement error, repeat the process (1)-(3) three times, and calculate the average value as the final experimental result.

TABLE II. GEOMETRICAL PARAMETERS AND PHYSICAL PROPERTIES FOR FLEXIBLE MANIPULATOR ARM IN THE EXPERIMENTS

Inner Diameter (mm)	8.8
Outer Diameter (mm)	10
Length of the Timoshenko element (mm)	1.67
Width of the Timoshenko element (mm)	1
Height of the Timoshenko element (mm)	1.35
Yong's Modulus (E) (Pa)	6e10
Destiny of material (kg/m3)	6.45e3
Poisson ratio	0.3

After the points are all measured by the laser tracker, the line connecting the two points in each deformation is built by the software of the laser tracker. The angle between the lines can be calculated by the laser tracker software, which represents the deformation angle in different driven load.

During the experiments, only one single side wire is actuated and the other one is under a free state. The discrete wire tension is acted on the driven wire from 0 to 14N in the experiments. Fig. 10 shows the mechanics model and the experiment results of two continuum manipulators with different number of notches. It can be seen that the result of mechanics matches the experimental result very well.

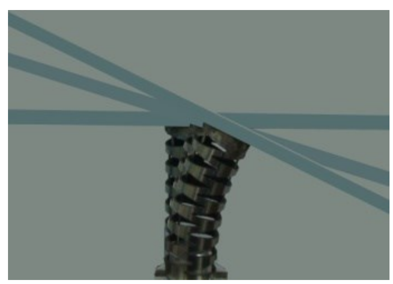

Fig. 8 Deformation of 6 V-shape units prototype piece under different loads shows the effectiveness of this type of continuum arm.

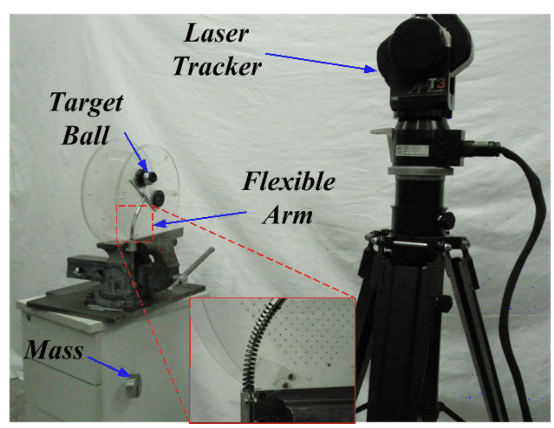

Fig. 9 The experimental test of the prototype continuum arm.

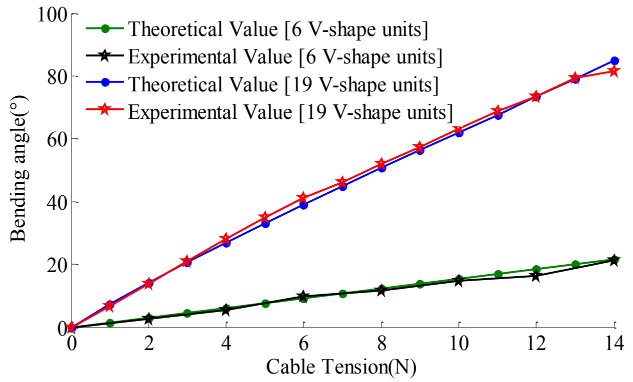

Fig. 10 The comparison results for bending angle between experiment and mechanics model analysis.

VI. Conclusion and Future work

In this paper, a mechanics-based kinematic model is proposed for the flexible manipulator arm with triangular notches. The proposed mechanics model is based on the improved Timoshenko's beam theory, which decomposes the whole dexterous manipulator into several V-shape units for the deformation analysis. The distributed force caused by the driven wire is simultaneously considered in the model. Finally, the proposed model is validated through the comparison between the theoretical analysis data and prototype experiment results. The model and the method proposed in this paper are generic, which can be extended for analyzing this notched type of flexible manipulator arm. It provides the fundamental for model-based position control of continuum robots under external loads. Our future work will be dedicated to optimization of the manipulator geometry and extending the proposed approach to spatial bending with multiple wires.

Acknowledgment

This research is supported in part by the National Natural Science Foundation of China under Grant No.61175078, State Key Lab Self-planned Project under Grant No. SKLRS201001A04 and HIT Overseas Talents Introduction Program. The authors also would like to thank all the engineers in the laboratory for their helps during the prototyping and experiments.

References

[1] G. Robinson and J. B. C. Davies, "Continuum robots. A state of the art," in Proceedings of the IEEE International Conference on Robotics and Automation, 1999, pp. 2849-2854.

[2] R. J. Webster, III and B. A. Jones, "Design and kinematic modeling of constant curvature continuum robots: A review," Int. J. Robot. Res., Vol. 29, pp. 1661-1683, 2010.

[3] G. Dogangil, B.L. Davies, F. Rodriguez y Baena, and et al., "A review of medical robotics for minimally invasive soft tissue surgery," Proc. IMechE Vol.224 Part H:J. Engineering in Medicine, 2010, pp. 653-679.

[4] J. Dumpert, A.C. Lehman, N.A. Wood, and et al., "Semi-autonomous surgical tasks using a miniature in vivo surgical robot," in the 31st Annu International Conf of the IEEE EMBS,2009, pp. 266-269.

[5] N. Suzuki, A. Hattori, K. Tanoue, S. Ieiri, and et al., "Scorpion shaped endoscopic surgical robot for NOTES and SPS with augmented reality functions," MIAR 2010, LNCS 6326, pp. 541-550, 2010.

[6] J. N. Ding, K. Xu, R. Goldman, and et al., "Design, simulation and evaluation of kinematic alternatives for insertable robotic effectors platforms in single port access surgery," in Proceedings of the IEEE International Conference on Robotics and Automation, 2000, pp. 618-621.

[7] K. Xu, R. E. Goldman, J. Ding, P. K. Allen, D. L. Fowler, and N. Simaan, "System design of an insertable robotic effector platform for single port access (SPA) surgery," in Proceedings of the IEEE/RSJ International Conference on Intelligent Robots and Systems, 2009, pp. 5546-5552.

[8] K.Harada, B. Zhang, S. Enosawa, T. Chiba, and et al., "Bending laser manipulator for intrauterine surgery and viscoelastic model of retal rat tissue," in Proceedings of the IEEE International Conference on Robotics and Automation, 2007, pp. 611-616.

[9] B. Jones and I. D. Walker, "Kinematics for multisection continuum robots," IEEE Transactions on Robotics, vol. 22, no. 1, pp. 43-55, 2006.

[10] P. E. Dupont, J. L. B. Itkowitz, and E. Butler, "Design and control of Concentric-Tube robots," IEEE Transactions on Robotics, Vol. 26, No. 2, pp. 209-225, 2010.

[11] J. Lock, G. Laing, M. Mahvash and P. E. Dupont, "Quasistatic modeling of concentric tube robots with external loads," in Proceedings of the IEEE/RSJ International Conference on Intelligent Robots and Systems, Taiwan, 2010, pp.2325-2332.

[12] K. Xu, N. Simman, "An investigation of the intricsic force sensing capabilities of continuum robots," IEEE Transactions on Robotics, Vol. 24, No. 3 pp. 576-587, 2008.

[13] B. Zhang, Y. Kobayashi, Y. Maeda, T. Chiba, and M.G. Fujie, "Development of 6-DOF wire-driven robotic manipulator for minimally invasive fetal surgery," in IEEE International Conference on Robotics and Automation, 2011, pp. 2892-2897.

[14] M. Neto, A. Ramos, and J. Campos, "Single port laparoscopic access surgery," Tech. Gastrointestinal Endosc., vol. 11, pp. 84-93, 2009.

[15] M. D. Kutzer, M. Segreti, S. M. Brown, et al., "Design of a new cable-driven manipulator with a large open lumen: Preliminary applications in the minimally-invasive removal of osteolysis," in Proceedings of IEEE International Conference on Robotics and Automation, 2011, pp. 2913-2920.

[16] D. Trivedi, A. Lotfi, and C. Rahn, "Geometrically exact models for soft robotic manipulators," IEEE Transactions on Robotics, vol. 24, pp. 773-780, 2008.

[17] R. J. Webster III, A. M. Okamura, and N. J. Cowan, "Toward active cannulas: Miniature snake-like surgical robots," in Proceedings of IEEE/RSJ International Conference on Intelligent Robots and Systems, 2006, pp. 2857-2863.

[18] D. C. Rucker, R, J. Webster, "Statics and dynamics of continuum robots with general tendon routing and external loading," IEEE Transactions on Robotics, vol, 27, no. 6, pp. 1033-1044, 2011.

[19] D. B. Camarillo, C. F. Milne, C .R. Carlson, et al., "Mechanics modeling of tendon-driven continuum manipulators," IEEE Transactions on Robotics, vol.24, no. 6, pp. 1262-1273, 2008.

[20] Y. Bailly, Y. Amirat, and G. Fried, "Modeling and control of a continuum style microrobot for endovascular surgery," IEEE Transactions on Robotics, Vol. 27, No. 5, pp. 1024-1030, 2011.

[21] Yunhua Luo, "An efficient 3D timoshenko beam element with consistent shape functions," Adv. Theor. Appl. Mech., Vol. 1, 2008, no. 3, pp. 95-10.